ARTICLE NO. 80-4022

J80-079

Surface Disintegration and Bubble Formation in Vertically Vibrated Liquid Column

20006
20020
30020

Hiroyuki Hashimoto* and Seiichi Sudō†
Tōhoku University, Sendai, Japan

A comprehensive theoretical and experimental study is made of free surface sloshing in a vertically oscillating cylindrical container at high frequency with emphasis placed upon the dynamics of the gas-liquid interface. The formation of liquid drops ejected from the free surface, gas entrainment in the liquid, and bubble motions are studied experimentally. It is found that the input acceleration required for surface disintegration is dominated by the liquid depth, and that the scales and the trajectory heights of the drops are dominated by the types of surface disintegration mechanisms achieved. An analysis is made of the gas entrainment caused by impacts of the drops upon the free surface. The behavior of the gas-liquid interface during the impacts and bubble formations are analyzed numerically. Theories for the vertical motions of the pulsating bubbles and their mutual attractive motions are also developed. Theoretical results agree approximately with the experimental results. Bubble motions in vertically vibrating liquid columns could be estimated quantitatively by the numerical results.

Nomenclature

C = velocity of pressure wave in two-phase mixture
C_D = drag coefficient
D = diameter of container
d = diameter of drop or bubble
E = Young's modulus
F = force
f = frequency
g = acceleration of gravity
H = liquid depth
L = wavelength
n = polytropic index
P = pressure
$\bar{P}$ = dimensionless pressure, $\bar{P}=P/(g\rho_\ell H)$
R = radius of container, or radius of bubble
$\bar{R}$ = representative radius of bubble, R at $t=0$
r = radial coordinate, or distance between two bubbles
S = thickness of container wall
T = trajectory height, or period
t = time
$\bar{U}$ = average bubble velocity for a given period of input oscillation
V = bubble volume
u,v = velocity components corresponding to r and z
X = input displacement of container
x = distance between two bubbles, $x=r/\bar{R}$
$\bar{Z}$ = dimensionless axial coordinate, $\bar{Z}=z/H$
z = axial coordinate taken downward from free surface
α = dimensionless acceleration, $\alpha=X\omega^2/g$
$\bar{\alpha}$ = void fraction
ν = kinematic viscosity
ρ = density
ω = angular frequency
ϕ = dimensionless frequency, $\phi=\omega H/C$

Subscripts

b = bottom of container
c = cluster
d = surface disintegration
e = equilibrium
g = gas
i = initial
ℓ = liquid
m = mutual attraction
s = spray excited
v = vertical direction

Received March 30, 1979; revision received July 16, 1979.

Index categories: Space Processing; Wave Motion and Sloshing; Hydrodynamics.

*Professor of Dynamics of Interface, Institute of High Speed Mechanics.

†Research Assistant of Dynamics of Interface, Institute of High Speed Mechanics.

Introduction

EXTENSIVE investigations have been made and reported of liquid sloshing and its influence on the overall dynamics of liquid fuel rockets, spacecraft, and many other moving vehicles.[1] Several similar problems are associated with the oscillation of liquid in containers during earthquakes,[2] the mixing of gas and liquid in a tank, chemical engineering applications,[3] and the effect of bubble vibration in acoustic cavitation.[4]

These previous studies have shown that as the input amplitude of a vertical oscillating container is increased, a point is reached at which the wavelets on the free surface disintegrate and form a spray of liquid particles. This strong instability of the surface causes gas entrainment in the liquid. Since drawing gas into the liquid could affect seriously the hydrodynamic performances of flow through the container and pumping systems connected to the container, the importance of gas-liquid interface sloshing is well-recognized.

Large amplitude waves and spray particles ejected from the free surface have been investigated theoreticlly and experimentally.[5-8] The motions of gas bubbles and bubble clusters in vibrated liquid columns have also been investigated theoretically and experimentally.[9-16] Mutual attractions between bubbles in an acoustic pressure field have been investigated theoretically and experimentally.[17-19] While these reports show the existence of spray-excited waves at the free surfaces and the motion of the bubbles in vibrated liquid columns, little information is currently available on the hydrodynamical mechanism of gas entrainment from the turbulent interface with spray particles. Further research into bubble formation and bubble behavior in vibrated liquid columns would be helpful.

The purpose of the present paper, therefore, is to present a comprehensive experimental and theoretical study of gas-

liquid surface sloshing in a vertically excited cylindrical container at high frequency with emphasis placed chiefly upon the dynamics of interface, and to investigate the behavior of ejected liquid drops, gas entrainment, and gas bubble motions in more detail.

Experimental Apparatus

A block diagram of the apparatus is shown in Fig. 1. An acrylic plastic cylinder, 500 mm long, 8 mm thick, and 184 mm in diameter containing water was excited longitudinally and sinusoidally by an electrodynamic shaker. (A few tests were conducted with a container 500 mm long, 6 mm thick, and 119 mm in diameter.) The shaker was operated at up to 20 mm amplitude and 1000 Hz frequency by an automatic control system, which consisted of an oscillator, servo-controller, and programmer.

The container displacement was measured by accelerometers monitored simultaneously on a dual trace oscilloscope and an electromagnetic oscilloscope. The frequency was measured by a digital counter. The displacement of the liquid-free surface was measured by an electrical probe and by an optical cathetometer, both of which are accurate to 0.01 mm. The motions of the liquid surface, liquid drops, and gas bubbles were photographed by a high beam stroboscope-streakcamera system.

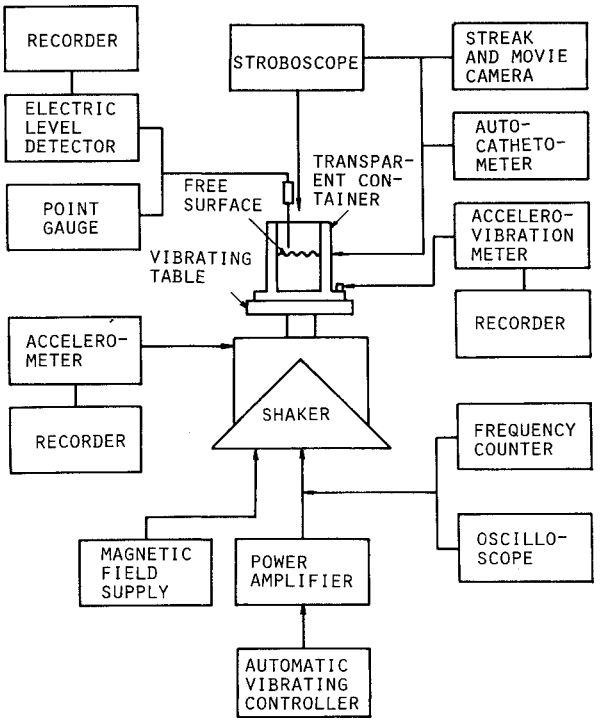

Fig. 1 Block diagram of apparatus.

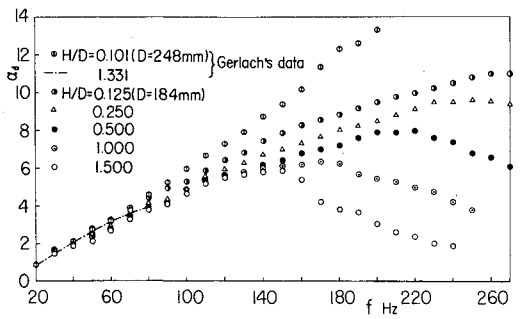

Fig. 2 Relation of dimensionless input acceleration α_d to frequency f for threshold of spray.

Experimental Results

Surface Disintegration

As input amplitude increased slowly from zero at a given frequency, the free surface in the container usually responded harmonically in a symmetric fashion; eventually, a point was reached at which the free surface exhibited the well-known ½ subharmonic response of individual wavelets all over the free surface. Increasing the input amplitude further caused the crests of the ½ subharmonic wave to disintegrate and form liquid spray particles.

Figure 2 shows the threshold input acceleration α_d for spray formation as a function of the input frequency f for several liquid depths, H/D (where α_d is the dimensionless acceleration required for the surface disintegration). From the figure, it is seen that α_d is a maximum for certain frequencies, f. The input amplitude X_d required for the surface disintegration decreases with increasing f. This probably results from the fact that the ½ subharmonic waves are more likely to switch to other modes and to interact with each other for larger f. Furthermore, former theoretical results[6] reveal that as f is increased, the unstable regions for various wave modes overlap considerably. It is also seen from Fig. 2 that the larger the dimensionless depth H/D is, the smaller α_d is. This decrement of α_d as a function of H/D increases with f. The reason for this is that as the input frequency f increases and approaches the natural frequency of liquid acoustic wave in the cylindrical container (and the larger H/D becomes, the smaller this natural frequency becomes), the liquid displacement produced by the pressure wave propagating in the liquid column becomes larger, with the liquid particles near the free surface especially disturbed, so the surface waves tend to become unstable.

Liquid Drop Formation and Trajectory Height

Figure 3 is a photograph of the gas-liquid interface for a cylindrical container oscillated longitudinally at $\alpha = 1.3$. The mechanisms of liquid drop formations can be classified roughly into the following three groups:

1) Larger drops, formed regularly as a result of tearing of a crest of ½ subharmonic wave. The average diameter of these drops decreases with increasing f. This follows from the experimental fact that the drop diameter d is roughly proportional to the wavelength L of the ½ subharmonic wave, and L decreases with increasing f. From our tests, the relative diameter d/L is approximately $0.25 \sim 0.35$, for $f > 50$ Hz.

2) Small drops, formed as a result of the breaking up of a sufficiently slender wave crest.

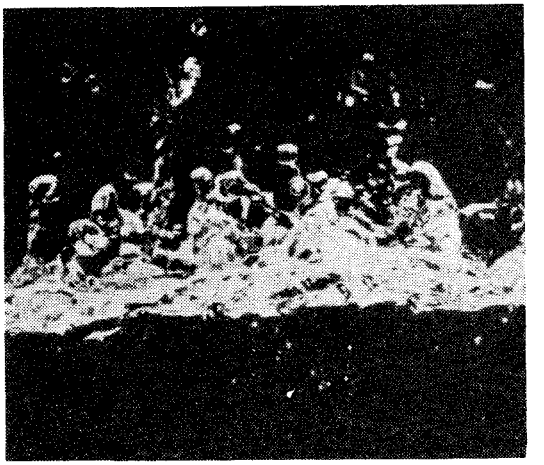

Fig. 3 Photograph of representative liquid drop formations, $H/D = 0.75$, $f = 20.0$ Hz, $\alpha = 1.41$.

3) Other small drops, formed as a result of the disintegration of larger drops when they fall back onto the free surface, or when a slender crest of a ½ subharmonic wave inclines and impacts the free surface.

The scales of the liquid drops therefore correspond roughly to the types of the surface disintegration mechanisms produced by this vibration.

The trajectory heights and the number of liquid drops above the free surface were observed to depend on the input amplitude and frequency. Figure 4 shows a sketch (resulting from several photographic exposures) of the concentration distribution of liquid drops above the free surface. The shades of the droplet layers indicate roughly the following three classifications. The darkest layer is the turbulent gas-liquid interface (layer 1). The somewhat more lightly shaded layer includes the many large overlapping drops (layer 2). The relatively light upper layer (layer 3) is the scattered small drops. The drops in all layers jump out of the free surface approximately uniformly and vertically except in the neighborhood of the container wall, unless a large amplitude spray-excited lower mode wave is generated (see the next section).

Figure 5 shows the relation of trajectory heights T_1, T_2, and T_3 for the three layers to the input accleration α within the region from the threshold of surface disintegration to the threshold of spray-excited waves. From the figure, it is evident that T_1, T_2, and T_3 increase with α. The derivative $dT/d\alpha$ for all layers decreases with increasing f, and $dT_2/d\alpha$ and $dT_3/d\alpha$ are larger than $dT_1/d\alpha$. Layer 1 consists mainly of the peak-to-peak displacement of the large amplitude ½ subharmonic waves. When T_1 is sufficiently larger than the input amplitude X, the following relation is obtained: $T_1 \cong 32X$. The drop scale in layer 2 is approximately uniform and larger than in layer 3. This implies that most of layer 2 consists of the drops which are formed regularly as a result of tearing off the crests of ½ subharmonic waves. Layer 3 consists of some small drops which are formed by breaking up of the slender crests and by splashing of larger drops; T_3 corresponds to the maximum trajectory height of these drops.

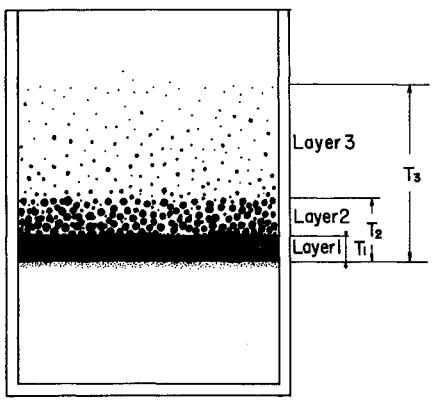

Fig. 4 Schematic sketch of liquid drops showing distribution of concentration above free surface.

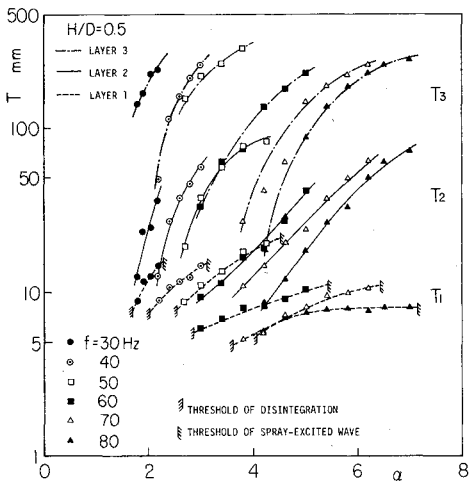

Fig. 5 Trajectory heights of drops.

Spray-Excited Waves

By increasing the input accleration at a given f, the number of drops impacting the free surface increases. Sometimes the free surface is excited into one of its lower modes, possibly at large amplitudes, by the droplet impacts. The first few modes of these large amplitude oscillations were easily excited. Figure 6 shows the threshold of these stable lower modes of spray-excited waves. Increasing the input acceleration α for a given f excited these modes in the order: (0, 1), (2, 1), and (1, 1). The larger H/D was, the smaller was the input acceleration α_s necessary to cause spray excitation. The amplitudes of these waves were very sensitive to changes in α at a given frequency. Although the interface of the spray-excited wave was more turbulent than that of the ½ subharmonic waves, with clusters of small liquid drops often observed on the interface, the wave frequency was approximately equal to the natural slosh frequency determined numerically from the assumption of a smooth free surface wave.

Gas Entrainment from Free Surface

When a lot of liquid impacted the free surface, many small gas bubbles were observed to form uniformly close to the free surface. Most of the bubbles were smaller than 2.5 mm in diameter. The air entrainment mechanism appeared to be very complex and to include several patterns. The bubble diameter differed roughly with each pattern. One of the most representative patterns appears to be as follows: When a drop from layer 2 impacts the free surface, a large crater is formed

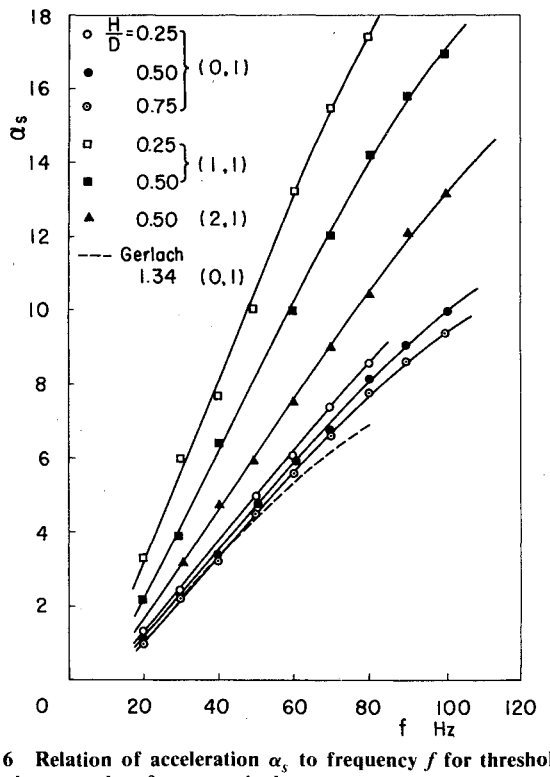

Fig. 6 Relation of acceleration α_s to frequency f for threshold of stable lower modes of spray-excited waves.

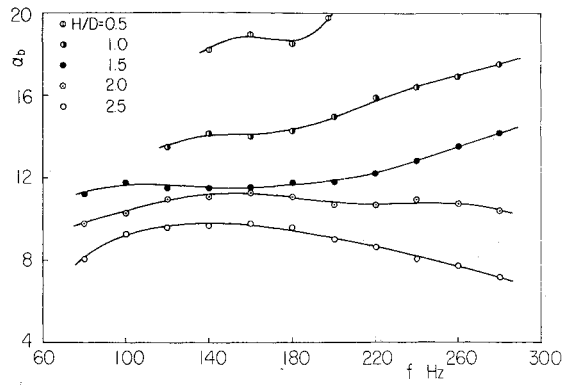

Fig. 7 Relation of α_b to f for condition that bubble remains at bottom of container.

momentarily on the free surface. If another small drop from layer 3 impacts the bottom of the crater just when the depth of the crater becomes maximum, a narrow but deep gas cavity is formed at the center of the crater. The upper part of the cavity is closed by the flow of the liquid around the first crater and immediately a spherical gas bubble is formed by the action of the surface tension (cf. analytical treatment). The higher the input frequency is, the smaller are the bubbles. The bubble scale is approximately proportional to the liquid drop scale and the wavelength of the surface wave. Of course, gas bubbles can also be formed by other mechanisms, such as air being drawn in from the violent surface motion.

Motions of Bubbles

Due to forces produced by the liquid pressure gradient, vertical bubble motions were observed in the vibrated liquid column. Such bubble motions depend chiefly upon the buoyancy force produced by both gravity and vertical excitation acceleration, since other bubble forces are generally negligible. The bubbles can become negatively buoyant by the excitation acceleration during each period of the oscillation and thus sink to the container bottom. If the stability condition $(d\alpha/dz>0)$[12] is satisfied at the equilibrium position where the total force during one period is zero, the bubble remains suspended at the equilibrium position. If α is so large that many bubbles are entrained in the liquid, the bubbles sink and reach the container bottom. Figure 7 shows the required relation between f and α_b so that any bubble that reaches the container bottom remains there. The larger H/D is, the smaller the required α_b is. Such a tendency is similar to the relation of α_d to H/D at the threshold of surface disintegration (see Fig. 2). This is consistent with the fact that the air entrainment is caused by the surface sloshing accompanying the liquid drop impact.

A mutual attraction between bubbles and a migration of bubbles to a solid wall were also observed. Such bubble behavior as well as the vertical motion in a vibrating liquid column[19] are often referred to as motions produced by Bjerknes' force. Two bubbles in a vibrating liquid column attract each other, and their relative velocities increase with the decreasing distance between them. The effect of the solid wall on the bubble in the vibrating pressure fields could be estimated in the same manner as the mutual attraction of two bubbles, because the solid boundary condition in an ideal flowfield is satisfied analytically by an image source and sink system of the same phase as the pulsating bubble. Ultimately, all of the bubbles gathered around a point adjoining the container wall. Once two bubbles approached so close that their spherical form was deformed; often they bounced. This could be caused by the unsymmetrical pressure distributions around the bubbles as a result of the change of the surface tension force on the liquid film between the bubbles. The large majority of bubbles did not coalesce to make a cluster as

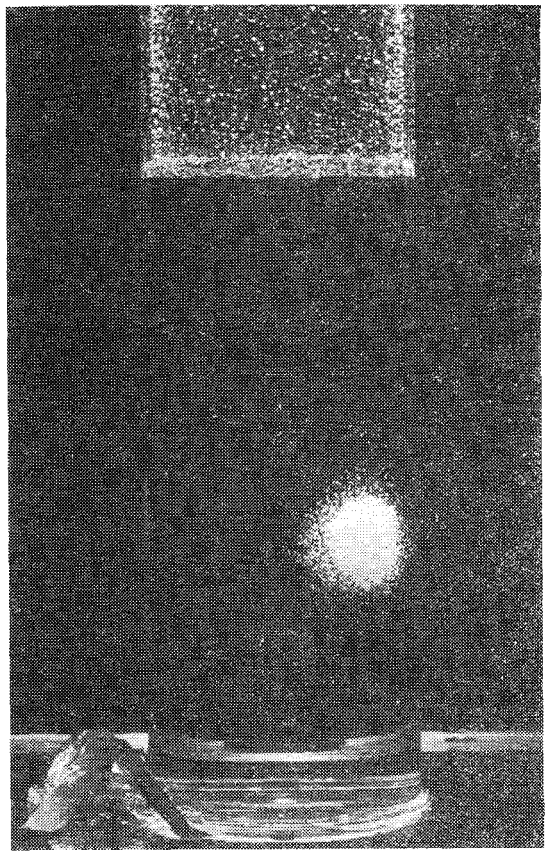

Fig. 8 Photograph of bubble cluster.

shown in Fig. 8. The cluster moved according to the input acceleration and pulsated as a whole. The larger the input amplitude X was, the more violently it pulsated. Furthermore, the location where the cluster remained was affected by the location of the container wall having the maximum deflection, as well as the equilibrium position as already stated. Figure 9 shows the statistical average diameters d_c/D of individual bubbles in a cluster. The smaller α is at f=constant, the larger are the individual bubble diameters.

Theoretical Analysis

Gas Entrainment

Since it is difficult to clarify in detail the flow patterns of gas entrainments solely by experiment, the gas-liquid interface behavior accompanying gas entrainment was analyzed by the Simplified Marker and Cell (SMAC) method.[20] We computed the following representative example: A small drop impacts the bottom of a crater formed previously by the impact of another large drop; that is, two different size drops fall from different heights above the free surface. Assuming the flowfield to be axisymmetric, the equation of continuity and the Navier-Stokes equations in cylindrical coordinates are:

$$\frac{1}{r}\frac{\partial ru}{\partial r}+\frac{\partial v}{\partial z}=0 \tag{1}$$

$$\frac{\partial u}{\partial t}+\frac{1}{r}\frac{\partial ru^2}{\partial r}+\frac{\partial uv}{\partial z}=-\frac{1}{\rho}\frac{\partial p}{\partial r}+\nu\frac{\partial}{\partial z}\left(\frac{\partial u}{\partial z}-\frac{\partial v}{\partial r}\right) \tag{2}$$

$$\frac{\partial v}{\partial t}+\frac{1}{r}\frac{\partial ruv}{\partial r}+\frac{\partial v^2}{\partial z}=-\frac{1}{\rho}\frac{\partial p}{\partial z}+g-\frac{\nu}{r}\frac{\partial}{\partial r}\left[r\left(\frac{\partial u}{\partial z}-\frac{\partial v}{\partial r}\right)\right] \tag{3}$$

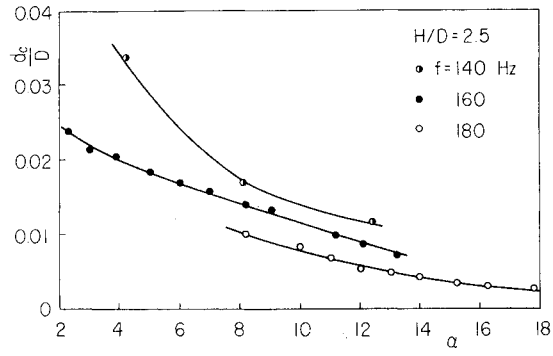

Fig. 9 Statistical average diameter d_c/D of individual bubble in a cluster for a given α, $D=119$ mm.

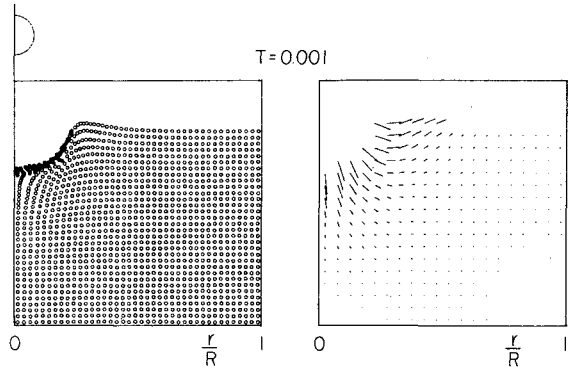

Fig. 10 Position of particles and velocity vectors at $t=0.001$ s after drop impacts onto the still free surface.

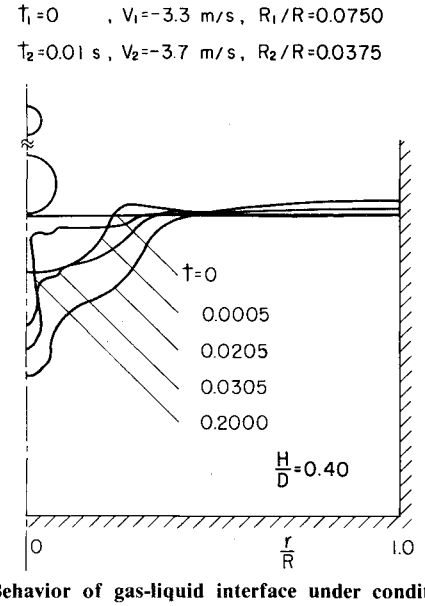

Fig. 11 Behavior of gas-liquid interface under condition: $t_1=0$, $v_1=3.3$ m/s, $R_1/R=0.0750$, $t_2=0.01$ s, $v_2=-3.7$ m/s, $R_2/R=0.0375$.

A stationary network of rectangular cells is utilized to divide the calculational region into a finite number of elements with which the fluid variables are associated. The cycle begins with reflagging. It is necessary to check each cycle to see if the cell flags need adjusting. The finite-difference equations for momentum and pressure are solved over the mesh of calculational cells by an iterative technique. Marker particles for fluid elements are moved through the cells to appropriate new locations. Boundary condition values and time counters are adjusted in such a way that the next cycle can begin.

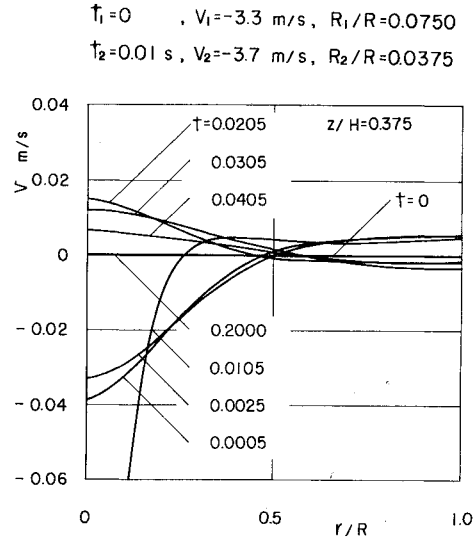

Fig. 12 Distribution of liquid velocities under the same conditions at Fig. 11.

Figure 10 shows an example of the numerical results for particle positions and velocity vectors in the liquid, at intervals of $t=0.001$ s after the first large drop impacts the quiescent liquid surface. The particles in the figure initially had been uniformly located in all liquid regions. Figure 11 shows the change in the free surface with time. The initial condition is that a drop impacts at $t_1=0$ with initial velocity $v_1=3.3$ m/s, and another smaller drop impacts at $t_2=0.01$ with initial velocity $v_2=3.7$ m/s. The figure shows the following liquid motion: The liquid near the crater surface begins to return upward a short time after the first drop impacts. Since another small drop impacts onto the center of the crater bottom at this time, the upper part of the deep gas cavity made by the small drop becomes very narrow and then the gas is entrained in the liquid. Figure 12 shows the change in the liquid velocity distribution in the container with time for the same conditions as Fig. 11. Of course, when the container is vibrating with a large amplitude, the behavior of the gas-liquid interface becomes more turbulent and complex. Furthermore, to clarify the pattern in more detail, the effects of stronger drop impacts, unsymmetrical drops and free surface interactions, different time intervals between falling drops, and so on should be considered. But one of several mechanisms of gas entrainment from the free surface has been clarified further theoretically by this sample of numerical results.

Vertical Motion of Bubble

The analysis is based on the following assumptions: 1) A bubble is completely immersed in incompressible and inviscid liquid, and executes a spherically symmetric pulsation; 2) the container is always excited sinusoidally and vertically; 3) the frequency of the input oscillation is much smaller than the bubble resonant frequency and the bubble radius is much smaller than the wavelength of the pressure wave throughout the liquid.

If the smaller terms involving the bubble mass and the bubble acceleration are neglected,[12] the time average momentum balance for the bubble motion of a given period T, and the relation between the bubble volume and the pressure, are shown approximately by:

$$-\frac{1}{T}\int_0^T V\frac{\partial P}{\partial z}\,dt-\frac{\rho_\ell}{2T}\int_0^T AC_D\bar{U}_v^2\,dt=0 \tag{4}$$

$$P_g V^n = P_{g0} V_0^n \tag{5}$$

where subscript 0 shows the standard state. C_D is the coefficient of the hydrodynamic drag on the bubble expressed by:

$$V=\frac{4}{3}\pi R^3,\quad A=\pi R^2,\quad C_D=27\left(\frac{2\bar{U}_v R}{\nu}\right)^{-0.78} \tag{6}$$

When surface tension is neglected, the bubble pressure is shown by[1]:

$$P=P_0+\rho_\ell g z-X_0\rho_\ell C\omega\frac{\sin\left(\frac{\omega}{C}z\right)\sin(\omega t)}{\cos\left(\frac{\omega}{C}H\right)} \tag{7}$$

$$C^2=\frac{1}{\left\{\bar{\alpha}\rho_g+(1-\bar{\alpha})\rho_\ell\right\}\left\{\frac{1-\bar{\alpha}}{\rho_\ell C_\ell^2}+\frac{\bar{\alpha}}{\rho_g C_g^2}+\frac{D}{SE}\right\}} \tag{8}$$

Considering the case $[\alpha\sin(\phi\bar{Z})]/[\phi(\bar{P}_0+\bar{Z})\cos\phi]\ll 1$ (higher order terms are negligible), Eq. (9) is obtained from Eqs. (5-8) as follows:

$$-\frac{1}{T}\int_0^T V\frac{\partial P}{\partial z}=-\rho_\ell g V_0\left(1+\frac{1}{2n}\frac{\alpha^2}{\cos^2\phi}\frac{\sin(\phi\bar{Z})}{\phi(\bar{P}_0+\bar{Z})}\right.$$
$$\times\left\{\frac{\sin(\phi\bar{Z})}{\phi(\bar{P}_0+\bar{Z})}\frac{(1+n)}{2n}-\cos(\phi\bar{Z})\right\}\left\{1+\frac{1}{8}\left(1+\frac{1}{n}\right)\right.$$
$$\left.\left.\times\left(2+\frac{1}{n}\right)\left(\frac{\alpha}{\cos\phi}\frac{\sin(\phi\bar{Z})}{\phi(\bar{P}_0+\bar{Z})}\right)^2\right\}\right) \tag{9}$$

The vertical velocity of the bubble U_v during a given period $T=1/f$ of the input oscillation is constant within the desired accuracy because U_v is slowly varying and can be evaluated at a representative value $\bar{U}_v$ corresponding to the mid-interval time T. Thus, Eq. (10) is obtained as follows:

$$-\frac{\rho}{2T}\int_0^T AC_D\bar{U}_v^2\,dt=-\frac{27}{8}\rho_\ell\pi\nu^2\left(\frac{2\bar{R}\bar{U}_v}{\nu}\right)^{1.22}\left(1+\frac{1.22}{36n}\right.$$
$$\times\left(\frac{1.22}{n}+3\right)\left\{\frac{\alpha\sin(\phi\bar{Z})}{(\bar{P}_0+\bar{Z})\phi\cos\phi}\right\}^2\left\{1+\frac{1}{144}\left(\frac{1.22}{n}+6\right)\right.$$
$$\left.\left.\times\left(\frac{1.22}{n}+9\right)\left(\frac{\alpha\sin(\phi\bar{Z})}{(\bar{P}_0+\bar{Z})\phi\cos\phi}\right)^2\right\}\right) \tag{10}$$

From Eqs. (9, 10, and 4), the velocity $\bar{U}_v$ is shown in Eq. (11):

$$\bar{U}_v=\frac{\nu}{2\bar{R}}\left(\frac{32}{81}\frac{g\bar{R}^3}{\nu^2}\frac{\frac{1}{2n}\left(\frac{\alpha}{\cos\phi}\right)^2 S\{S-\cos(\phi\bar{Z})\}\{1}{1+\frac{1.22(1.22+3n)}{36n^2}\left(\frac{\alpha S}{\cos\phi}\right)^2\{1}\right.$$
$$\left.+\frac{(1+n)(1+2n)}{8n^2}\left(\frac{\alpha S}{\cos\phi}\right)^2\}-1}{+\frac{(1.22+6n)(1.22+9n)}{144n^2}\left(\frac{\alpha S}{\cos\phi}\right)^2\}}\right)^{0.82} \tag{11}$$

where $S=\sin(\phi\bar{Z})/[\phi(\bar{P}_0+\bar{Z})]$. Figure 13 shows numerical results for the downward velocity $\bar{U}_v$ obtained from Eq. (11). The dimensionless velocity $\bar{U}_v/\bar{U}_{vi}$ increases rapidly with dimensionless distance $\bar{Z}$ from the free surface, and is not much affected by the polytropic index n for α of order 20.

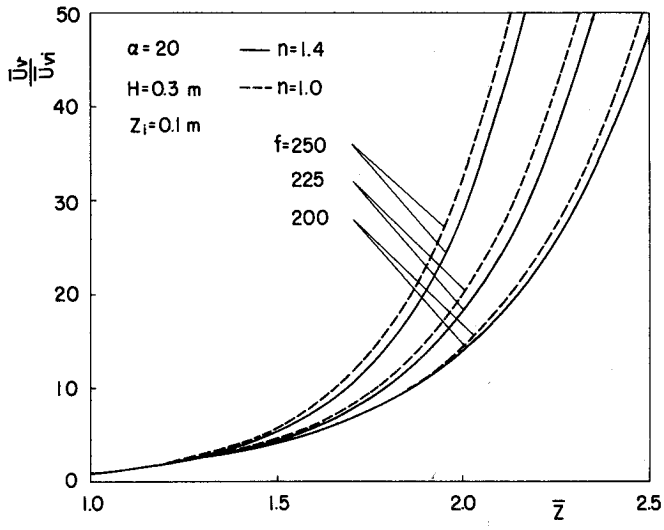

Fig. 13 Relation of vertical bubble velocity $\bar{U}_v$ to axial position $\bar{Z}$.

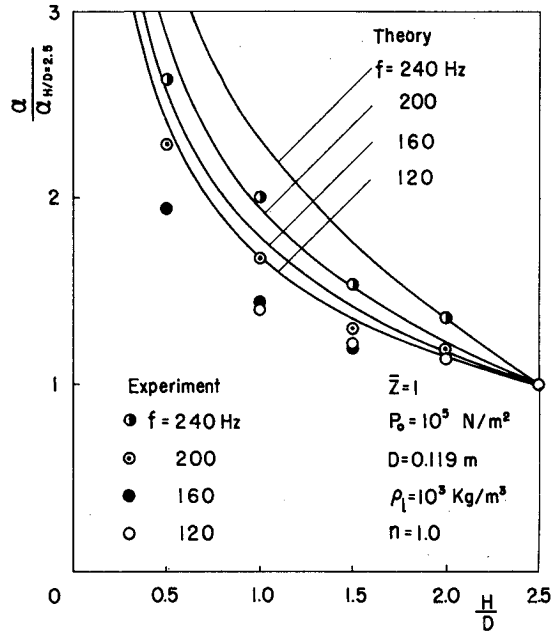

Fig. 14 Relation of input acceleration $\alpha_{\bar{Z}=1}$ to relative depth H/D.

If the bubble is pulsating at the equilibrium depth where the total buoyancy force due to gravity and input acceleration is zero, the acceleration α_e required for the equilibrium at the depth $\bar{Z}$ is expressed in Eq. (12), which follows from Eq. (11) and the condition $\bar{U}_v=0$:

$$\alpha_e=\frac{\cos\phi}{\sin(\phi\bar{Z})}\left(\left\{2n\phi(\bar{P}_0+\bar{Z})\tan(\phi\bar{Z})\right\}\right.$$
$$\left.\times\left\{1-\frac{(2-1/n)(1+n)\tan(\phi\bar{Z})}{4\phi(\bar{P}_0+\bar{Z})}\right\}\right)^{1/2} \tag{12}$$

If $n=1.0$, Eq. (12) agrees with the result obtained by Foster[12] (who treated the bubble motions only for the case of $n=1.0$).

Figure 14 shows the numerical relation between H/D (the variable in the theory is liquid depth H rather than H/D) and the equilibrium acceleration α_b required for equilibrium at the bottom $\bar{Z}=1$. The smaller H/D is, the larger α_b is. The theoretical results agree qualitatively with the experimental results. Differences might be caused by the unsuitable estimation of the pressure wave velocity and the lack of consideration of liquid flow inertia in the calculation.

Mutual Attraction of Two Bubbles

Based on the same assumptions as in the case of the vertical motion, a mutual attraction of two pulsating gas bubbles is analyzed. A bubble radius R at any time t is expressed in Eq. (13) by using Eqs. (5-7) as follows:

$$R=\bar{R}(1+a\sin\omega t)^m \tag{13}$$

where

$$m=-\frac{1}{3n},\quad a=\frac{-\alpha\sin(\phi\bar{Z})}{\phi(\bar{P}_0+\bar{Z})\cos\phi}$$

If the center of the pulsating bubble is positioned at the origin of a one-dimensional spherical coordinate system, the pressure P is expressed as:

$$P=\rho_l\left(\frac{R^2\ddot{R}+2R\dot{R}^2}{r}-\frac{1}{2}\left(\frac{R^2\dot{R}}{r}\right)^2\right) \tag{14}$$

Thus, the pressure P_r at a given radial coordinate r is expressed in Eq. (15) from Eqs. (13) and (14) as follows:

$$P_r=-\frac{\bar{R}^3}{r}\omega^2 ma\sin\omega t(1+a\sin\omega t)^{3m-2}(1-3ma\cos^2\omega t+a)$$

$$-\frac{\bar{R}^6}{2r^4}\omega^2m^2a^2(1+a\sin\omega t)^{6m-2}\cos^2\omega t \tag{15}$$

Considering that the actual pressure P is $P=\rho gZ_i+P_0+P_r$ at $z=z_i$ and that a is much smaller than unity, and neglecting terms of higher order than a^4, the average mutual attraction force

$$F_m=\frac{1}{T}\int_0^T V\frac{\partial p}{\partial r}\,dt$$

of a given period T is expressed as:

$$F_m=-2\pi(\bar{R}^2\omega am)^2\left(\frac{\bar{R}}{r}\right)^2\left(1+\frac{ma\omega^2\bar{R}^3}{\alpha gzr}+\frac{2}{3}\left(\frac{\bar{R}}{r}\right)^3\right) \tag{16}$$

If $n=1.0$, the first term of Eq. (16) is equal to the result of the linear analysis introduced by Crum.[19] Equation (16) is applicable to bubbles which pulsate with larger radial displacements than in the former investigations. Since the drag force and the momentum balance can be obtained in the same way as in Eq. (4), (9), and (10), a velocity $\bar{U}_m$ of the mutual attraction can be expressed in Eq. (17):

$$\frac{2\bar{R}\bar{U}_m}{\nu}=\left(\frac{2^4}{3^5}\left(\frac{\omega\bar{R}^2}{\nu}\right)^2\frac{a^2}{n^2x^2}-\frac{1+\dfrac{2}{3x^2}+\dfrac{\bar{R}^2a}{3nxzX_0}}{1+\dfrac{1}{270n^4}\dfrac{\bar{R}^2a}{zX_0}}\right)^{\frac{1}{1.22}} \tag{17}$$

Figure 15 shows the relation of $\bar{U}_m$ to x. The dimensionless velocity $\bar{U}_m/\omega\bar{R}$ increases greatly with decreasing x. If ϕ is a constant, the larger α is, the larger $\bar{U}_m/\omega\bar{R}$ is. $\bar{U}_m/\omega\bar{R}$ is much larger for $n=1.4$ than for $n=1.0$. From these results, it could be expected that bubbles pulsating with the same phase approach each other with velocities corresponding to r and a bubble cluster is easily formed in the liquid.

Since the actual free surface sloshing phenomena governing the dynamics of the gas-liquid interface are very complex, it is necessary to investigate them not only experimentally but also theoretically. These analyses and numerical results clarify bubble formation and motion in the liquid in greater detail.

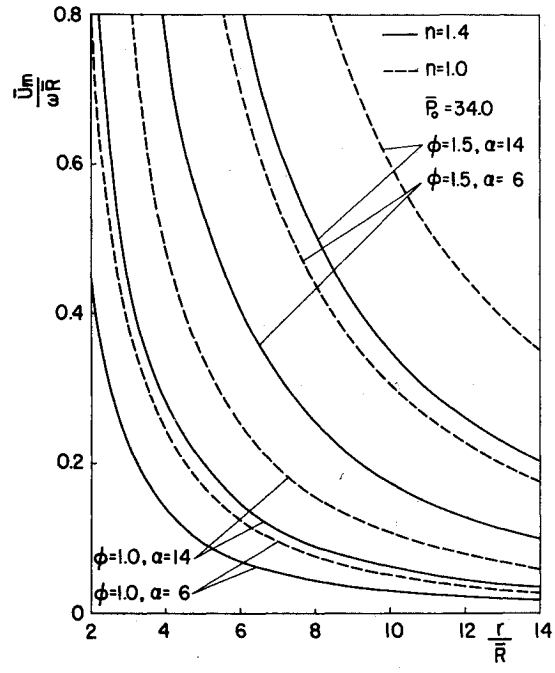

Fig. 15 Relation of mutual attractive velocity $\bar{U}_m$ to distance r between two bubbles.

Conclusions

1) The input acceleration α_d required for surface disintegration has a maximum at some input frequency f. The larger the dimensionless depth H/D is, the smaller α_d is.

2) The sizes of liquid drops ejected from the free surface correspond to the surface disintegration mechanisms; that is, larger drops near the free surface are formed regularly as a result of tearing off crests of ½ subharmonic waves, which is one of most representative drop formations.

3) The scales of all drops decrease with increasing f.

4) The trajectory heights of all drops increase with increases of the input displacement. The trajectory heights of some small drops formed by the breaking up of the sufficiently slender crests of ½ subharmonic waves are greater than those of the larger drops formed uniformly as a result of regular tearing.

5) The larger H/D is, the smaller is the input acceleration α_s necessary to generate the spray-excited lower mode waves.

6) A representative gas entrainment mechanism in the liquid is the impact of the drops onto the free surface. The behavior of the gas-liquid interface during gas entrainment was analyzed numerically.

7) An analytical solution for vertical motion of a pulsating bubble was developed. The vertical velocities and the equilibrium positions of the bubbles were determined as functions of the polytropic index. Theoretical results agreed approximately with the experimental results; that is, the smaller H is, the larger is the input acceleration α_b required for the bubbles to remain on the container bottom.

8) The mutual attraction of two bubbles which pulsate with large radial displacements was analyzed. The mutual attractive velocities of the bubbles were estimated numerically.

References

[1] Abramson, H. N., "The Dynamic Behavior of Liquids in Moving Containers," NASA-SP-106, 1966.

[2] Moody, F. J. and Reynolds, W. C., "Liquid Surface Motion Induced by Acceleration and External Pressure," *Journal of Basic Engineering, Transactions of ASME*, Ser. D. Vol. 94, Sept. 1972, pp. 606-612.

[3] Baird, M.H.I., "Resonant Bubbles in a Vertically Vibrating Liquid Column," *Canadian Journal of Chemical Engineering*, Vol.

41, April 1963, pp. 52-55.

[4]Prosperetti, A., "Nonlinear Oscillations of Gas Bubbles in Liquids: Transient Solutions and the Connection between Subharmonic Signal and Cavitation," *Journal of Acoustical Society of America*, Vol. 57, April 1975, pp. 810-821.

[5]Skalak, R. and Yarymovych, M. I., "Forced Large Amplitude Surface Waves," *Proceedings of Fourth United States National Congress on Applied Mechanics*, 1962, pp. 1411-1418.

[6]Dodge, F. T., Kana, D. D., and Abramson, H. N., "Liquid Surface Oscillations in Longitudinally Excited Rigid Cylindrical Containers," *AIAA Journal*, Vol. 3, April 1965, pp. 685-695.

[7]Gerlach, C. R., "Surface Disintegration of Liquid in Longitudinally Excited Containers," *Journal of Spacecraft and Rockets*, Vol. 5, May 1968, pp. 553-560.

[8]Perko, L. M., "Large-Amplitude Motions of a Liquid-Vapour Interface in an Accelerating Container," *Journal of Fluid Mechanics*, Vol. 35, Jan. 1969, pp. 77-96.

[9]Fritz, C. G., Ponder, C. A., Jr., and Blount, D. H., "Bubble Coalescence in a Longitudinally Vibrated Liquid Column," *Symposium on Cavitation in Fluid Machinery*, ASME Winter Annual Meeting, Chicago, Nov. 1965, pp. 148-161.

[10]Kana, D. D. and Dodge, F. T., "Bubble Behavior in Liquids Contained in Vertically Vibrated Tanks," *Journal of Spacecraft and Rockets*, Vol. 3, May 1966, pp. 760-763.

[11]Schoenhals, R. J. and Overcamp, T. J., "Pressure Distribution and Bubble Formation Induced by Longitudinal Vibration of a Flexible Liquid-Filled Cylinder," *Journal of Basic Engineering, Transactions of ASME*, Ser. D., Vol. 89, Dec. 1967, pp. 737-747.

[12]Foster, J. M., Botts, J. A., Barbin, A. R., and Vachon, R. J., "Bubble Trajectories and Equilibrium Levels in Vibrated Liquid Columns," *Journal of Basic Engineering, Transactions of ASME*, Ser. D, Vol. 90, March 1968, pp. 125-132.

[13]Gelger, G. E. and Kappler, G., "The Stabilization of Bubbles in Viscous Liquids in a Vertically Vibrated Tank," *Journal of Basic Engineering, Transactions of ASME*, Paper No. 67-FE-3, 1967.

[14]Pih, H. and Wu, C. G., "Experimental Studies of Vibration of Axially Excited Circular Cylindrical Shells Containing Fluid," *Journal of Engineering Industry, Transactions of ASME*, Ser. B, Vol. 91, Nov. 1969, pp. 1119-1127.

[15]Remenyik, C. J., "Bubbles, Steady Streaming and Surface Instability in Vibrated Liquid Columns," *Proceedings of 1970 Heat Transfer and Fluid Mechanics Institute*, Monterey, Calif., June 1970, pp. 62-73.

[16]Remenyik, C. J., "Surface Instability of Stationary Air Bubbles," *Proceedings of International Colloquium on Drops and Bubbles*, Vol. 2, Aug. 1974, pp. 592-605.

[17]Neppiras, E. A., "Subharmonic and Other Low-Frequency Emission from Bubbles in Sound-Irradiated Liquids," *Journal of Acoustical Society of America*, Vol. 46, Sept. 1969, pp. 587-601.

[18]Crum, L. A. and Eller, A. I., "Motion of Bubbles in a Stationary Sound Field," *Journal of Acoustical Society of America*, Vol. 48, July 1970, pp. 181-189.

[19]Crum, L. A., "Bjerknes Forces on Bubbles in a Stationary Sound Field," *Journal of Acoustical Society of America*, Vol. 57, June 1975, pp. 1363-1370.

[20]Amsden, A. A. and Harlow, F. H., "The SMAC Method: A Numerical Technique for Calculating Incompressible Fluid Flows," Los Alamos Scientific Laboratory, University of California, Rept. No. LA-4370, Feb. 1970.